Contemporary Mathematics
https://ojs.wiserpub.com/index.php/CM/

Research Article

Finite Element Multigrid Simulation of Natural Convection in Hybrid Nanofluids Within Isolated Cavity for Solar Energy Systems: A Machine Learning-Levenberg-Marquardt Approach

Hamayat Ullah[1], Muhammad Salim Khan[1], Zahir Shah[1*], Maria Alina Fălădău[2], Nahid Fatima[3], Muhammad Sarwar[3,4], Kamaleldin Abodayeh[3]

[1] Department of Mathematical Sciences, University of Lakki Marwat, Lakki Marwat, KPK, 28420, Pakistan
[2] Faculty of Engineering, Lucian Blaga University of Sibiu, Sibiu, 550024, Romania
[3] Department of Mathematics and Sciences, Prince Sultan University, Riyadh, 11586, Saudi Arabia
[4] Department of Mathematics, University of Malakand, Chakdara Dir (Lower), KPK, Pakistan
E-mail: Zahir@ulm.edu.pk

Received: 22 January 2026; **Revised:** 4 February 2026; **Accepted:** 10 February 2026

Abstract: This study examines magnetoconvective heat transfer in an enclosure filled with a hybrid nanofluid consisting of Multi-Walled Carbon Nanotubes (MWCNTs) and iron oxide (Fe_3O_4) nanoparticles, a configuration with strong relevance to solar thermal energy storage and management systems. The governing transport equations are solved using the Finite Element Method (FEM) implemented in COMSOL Multiphysics to analyze the coupled effects of buoyancy, magnetic field, and non-Newtonian rheology. The influence of key controlling parameters, namely the Rayleigh number (Ra), Hartmann number (Ha), and Casson parameter (β), is systematically investigated. The results reveal that increasing Ra significantly intensifies buoyancy-driven flow circulation, leading to a 36.54% enhancement in convective heat transfer. In contrast, stronger magnetic fields (higher Ha) suppress fluid motion and thermal transport by up to 47.91% due to Lorentz-force-induced damping. Furthermore, an increase in the Casson parameter promotes Newtonian-like behavior, reducing viscous resistance and resulting in a 48.96% improvement in heat transfer performance. These findings provide clear physical insight into the competing roles of buoyancy, magnetic control, and rheological effects in hybrid nanofluid systems. To support rapid prediction and parametric analysis, an Artificial Neural Network (ANN) surrogate model is additionally developed and validated against FEM data, demonstrating high predictive accuracy. FEM simulations are carried out using COMSOL Multiphysics, while the ANN model is implemented in MATLAB. Overall, the study offers both fundamental physical understanding and practical guidance for optimizing magnetically controlled hybrid nanofluid systems in solar energy applications.

Keywords: Natural convection, Multi-Walled Carbon Nanotube (MWCNT)-(Fe_3O_4)/water hybrid nanofluid, Artificial Neural Network (ANN), inverted T-shaped enclosure, Finite Element Method (FEM)

MSC: 65N30, 76D05, 68T07

DOI: https://doi.org/10.37256/cm.7220269157

Nomenclature

AR	Cavity obstruction ratio	MWCNTs	Multi-Walled Carbon Nanotubes
Fe_3O_4	Iron oxide	FEM	Finite Element Method
Ra	Rayleigh number	LM	Levenberg Marquardt
MSE	Mean Squared Error	PV/T	Photovoltaic-Thermal systems
MHD	Magnetohydrodynamics	Ha	Hartmann number
DOF	Degrees of Freedom	Nu_{avg}	Average Nusselt Number
k	Thermal conductivity	Abs_{Error}	Absolute Error
Rel_{Error}	Relative Error	L	Height of cavity
L_1	Width of cavity	Nu	Nusselt number
p	Pressure	Pr	Prandtl number
T	Temperature	u, v	Nondimensional velocity components
W	Length of cavity	β	Casson parameter
μ	Dynamic viscosity	ρ	Density
ANN	Artificial Neural Network	c	Cold
f	Fluid	h	Hot
nf	Nanofluid	α	Thermal diffusivity
ϕ	Volume fraction	β_1	Thermal expansion coefficient
W_1	Width of cavity	x, y	Coordinates

1. Introduction

Inverted T-shaped enclosure has significant benefits for solar energy systems, which mainly amplify natural convection and heat transfer within closed systems. Its unique geometry allows fluid flow, hence supporting the increase of thermal storage and distribution, especially when hybrid nanofluids are used. It is widely used in solar collectors, Photovoltaic-Thermal (PV/T) units, solar water heaters and thermal storage systems as it has a large heat transfer surface and allows stratification of the heat to the top part of the system to enhance the overall system output. The idea of the addition of solid particles to the fluids is not new and was introduced in the eighteenth century, but it was only with nanotechnology that the concept became practical. The hybrid nanofluids have been subject to increasing research attention in solar energy and thermal management practices due to their better thermophysical properties that enable them to have better heat transfer as compared to traditional fluids. Hybrid nanofluids are especially beneficial to Direct Absorption Solar Collectors (DASCs) and Parabolic Trough Solar Collectors (PTSCs) with increased efficiency in energy conversion and thermal stability. Hachicha [1] showed that the incorporation of hybrid nanofluids into PTSCs contributes to enhanced thermal efficiency caused by elevated absorption of solar energy and the transfer of heat by convection. Similarly, Huminic et al. [2] also gave experimental results that hybrid nanofluids inculcated into DASCs significantly increase the rates of heat transfer and maintain stable thermal functionality, which further confirms their usability in practical applications in solar systems. Kalsi et al. [3] provided a review of the recent advances in the production of hybrid nanofluids and their thermophysical properties, highlighting their extensive use in renewable energy and energy storage systems. Hannoura et al. [4] highlighted that the engineering importance of hybrid nanofluids in an energy system may be re-established through optimization of thermophysical properties of working fluids in solar collectors to optimize the rate of heat transfer and the working fluid efficiency. At the same time, Artificial Intelligence (AI) and neural network modeling techniques have become a strong predictive tool for intricate thermal and mass transfer in non-Newtonian fluids. Rehman et al. [5] used neural networks. Matori et al. [6] examined the natural convection of Multi-Walled Carbon Nanotube (MWCNT)-Fe_3O_4/water hybrid nanofluid in a Pi-shaped cavity with a heated obstacle, and their results demonstrated a tremendous increase in heat transfer owing to hybrid nanoparticles-discoveries that can be applied to receivers of solar cavity. An extensive numerical study of magnetohydrodynamic mixed convection in a lid-driven curvilinear cavity partly filled with a porous medium and using nanofluids.

Magnetohydrodynamics (MHD) has been extensively applied across various engineering domains, including electronics cooling, crystal manufacturing, and solar thermal systems, to improve heat transfer performance. MHD systems utilize magnetic fields to regulate fluid motion, thereby influencing thermal transport behavior. However, empirical investigations have shown that increasing the magnetic field strength, typically characterized by a higher Hartmann number (Ha), can adversely affect convective heat transfer. This phenomenon is attributed to the Lorentz force, which suppresses fluid motion and weakens natural convection, leading to a decrease in the convective heat transfer coefficient [7]. Kefayati and Tang [8] further demonstrated that an elevated Ha results in increased entropy generation due to the dampening of convective currents, underscoring the trade-off between flow stabilization and thermodynamic efficiency in MHD systems. Turkyilmazoglu et al. [9] studied Stokes flow of MHD in a cavity under the influence of parallel moving lids in a subsequent study and found that the applied magnetic field significantly inhibits the appearance of vortices and varies the internal flow structure. Alomari et al. [10] reported that the application of a magnetic field is a significant inhibitor of fluid motion but a considerable enhancer of thermal uniformity, although the porous layer significantly changes the circulation and heat-transfer patterns. Belhaj and Ben-Beya [11] analyzed natural convection of hybrid nanofluids in a square cavity with an internal obstacle in the form of an elliptical shape with a spatially varying magnetic field. Their findings revealed that hybrid nanoparticles have a strong effect on the heat-transfer performance while the aspect ratio of the obstacle and the magnetic-field gradients have overriding effect on the thermal response. Priyadharshini and Sowndharya [12] produced a predictive model that covered heat and mass transfer in magnetohydrodynamic Casson nanofluid flows that are relevant in the solar-collector applications; their results indicated that the intensity of the magnetic field, the concentration of nanoparticles and Casson rheology significantly impact thermal efficiency, showing considerable promise in optimising solar-thermal systems.

Turkyilmazoglu et al. [13] experimented with viscous MHD flow in a pipe with porous walls whereby more powerful magnetic fields augmented the resistance of the flow, axial velocity, but wall permeability impacted pressure gradients and the flow rate of the volume significantly. Negi et al. [14] studied hybrid-nanofluid flow, coupled mass and heat transfer in a multiphase environment under magnetohydrodynamic forces, in which hybrid nanoparticles significantly enhance heat transfer, but an increase in Hartmann number reduces velocity and changes concentration frame layers. David et al. [15] generalized the expanding-box formulation of Reduced Magnetohydrodynamics (RMHD) to the solar wind, which provides tuned theoretical tools to describe the expansion and turbulence development of the plasma as well as the global dynamics of the solar wind, and thus, enhances the modelling of solar-wind-driven MHD processes. Turkyilmazoglu et al. [16] studied the Magnetohydrodynamic (MHD) front stagnation-point flow and rear stagnation-point flow over a moving permeable flat plate and found out that fluid velocity is reduced and the skin friction is increased by the imposed magnetic field, and mass transfer is improved by wall permeability.

Izadi et al. [17] studied natural convection of a magnetizable hybrid nanofluid in a porous enclosure under two variable magnetic fields. They found that hybrid nanoparticles improve heat transfer, while stronger magnetic fields suppress convection and lower the Nusselt number. Higher Darcy numbers enhance flow circulation, and optimal heat transfer occurs at low magnetic-field strength. Much effort has been focused on the explanation of the effect of the interaction between nanofluids and porous materials on the performance of heat transfer under various thermal and thermal boundary conditions. Beckerman et al. [18], in one of the earliest studies, used the Brinkman-Forchheimer generalization of the Darcy model in their numerical study to analyse convection in a porous layer of a vertical cavity. They observed that the flow structure within the porous region is greatly affected by changes in the Darcy number, which has a powerful effect on heat and fluid movement within the cavity, as the permeability of the medium is determined by the Darcy number. Baytas et al. [19] examined the conduction and convection in a porous enclosure. They reported that the strength of the circulation within the cavity heavily relies on the ratio of thermal conductivity of fluid and solid matrix, meaning that the overall strength of the flow is controlled by the ability of the two phases to exchange energy effectively. On the same note, Chamkha and Ismael [20] examined the application of nanofluids in natural convection in porous enclosures with various Rayleigh numbers. Their findings showed that the nanofluids can significantly increase the heat transfer. Additionally, under low concentrations of Rayleigh numbers, the concentration of nanoparticles accumulating in the cavity enhances thermal conduction within the porous cavity because the thermal gradients is increased. Bourantas et al. [21] also studied the natural convection in a porous cavity, which has a localized heat source near the bottom wall and is

filled with a nanofluid. They found that the rate of heat transfer in the enclosure is greatly enhanced by the addition of nanoparticles. Hajipour and Dehkordi [22] conducted a numerical investigation of the mixed convection in a porous cavity of vertical orientation, which is partially filled with a metal foam soaked in a nanofluid. They found that mono-layering of nanoparticles in the base fluid enhances the thermal performance significantly. Specifically, a volume fraction of nanoparticles of 0.3% results in a significant increase in heat transfer of about 20 percent higher than that of traditional fluids. These results demonstrate the synergistic action of porous structures and nanoparticle dispersion in enhancing the convective heat transfer, and are expected to have an impact on solar collectors, electronics cooling, and sophisticated thermal management systems. Nguyen et al. [23] experimented on the motion of free convection of nanofluids in porous cavities at varying heating conditions. They discovered that the concentration of nanoparticles and the Rayleigh number has a significant impact on the heat transfer rates, with the heat transfer rate increasing notably with either parameter. Al-Zamily [24] and Sheikholeslami and Shamlooei [25] simulated TiO_2-water nanofluid in cavities with the transversal arrangement of porous layers. Their findings indicate that placing the heat source at the bottom part of the left wall favors more heat transfer.

Sushma et al. [26] analyzed the heat characteristics of hybrid nanofluids across nonlinear stretching surfaces through similarity transformations and Hermite wavelet approaches. The results of their study indicate the great impact of thermal radiation, showing that its implementation can drastically improve the heat transfer capability. In another companion paper, Ali et al. [27] also took into account the impact of magnetic fields on the flow in hybrid nanofluidics and found that a local minuscule magnetic field applied can control the development of vortex structures in such a way that the motion of fluid and its stability may be brought to the optimum. Mandal et al. [28] introduced a new W-shaped porous cavity and observed that it raises the effectiveness of the magnetohydrodynamic mixed convection of hybrid nanofluids to a large extent. This geometrical design provided better thermal performance as compared to other traditional designs. All these works emphasize the significance of geometrical designs of high order, thermal radiation, and magnetic field manipulation to promote heat transfer and flow control in hybrid nanofluid systems. AI is the application of intelligent computer technologies that can imitate human cognition and adaptive learning. Many technologies, such as natural language processing, machine vision, and expert systems, make use of it. Ordinary items such as search engines and smart appliances, as well as the innovative ones such as robotics, self-driving vehicles, and the creative industry, rely on artificial intelligence. The use of AI in solar energy aids solar panels to be more efficient through managing energy use, predicting the amount of sunlight, and detecting system malfunctions. This makes the solar power systems more reliable and effective.

Being a subdivision of artificial intelligence, the Artificial Neural Networks (ANNs), which are based on the biological neuron structure, are an imperative area of study since they can accomplish complex tasks such as pattern prediction and recognition. Although they were originally applied in ecological studies in the 1990s [29, 30], there has been a vast proliferation of their applications in recent decades, as a result of the growth in computational capacity and algorithm schemes [31]. ANNs have been shown to have great potential in the engineering field, particularly in the modeling of complicated physical processes. In this case, Shafiq et al. [32] applied ANNs to predict the properties of the boundary layers in a nonlinear isothermal flow in the nonlinear cylinders and paraboloids geometries, which were loaded with convective boundary conditions. Their findings underscore the possibility of ANNs having the ability to deal with immensely nonlinear problems. The ANNs methodology proposed by Mitusch et al. [33] are based on Partial Differential Equations (PDEs), where Finite Element Method (FEM) is applied to the entire process of training to ensure physical fidelity of machine learning approaches.

This mixed method would continue to follow the basic laws of physics but would increase the accuracy of the predictions. These ANN-based strategies are also finding useful applications in nanofluid research development since they are computationally efficient as well as provide physical insight. Alshare combined convolutional and recurrent neural networks to enhance its ability to categorize the heat movement in the solar collectors based on nanofluids. This proved correct since their model had improved the performance of prediction by 22% compared to the early techniques, which show that AI can assist solar systems to be more efficient. Similarly, Ahmadi et al. [34] employed different ANNs to determine the thermal conductivity and viscosity of the Fe_2O_3/water nanofluid. Among them, the Genetic Algorithm optimized Radial Basis Function (GA-RBF) was identified as the most successful one. These publications suggest that

ANNs are a versatile and dynamic tool that can be applied in the optimization of the nanofluid behavior, which is needed in the existing systems in terms of heat and energy control.

Though a lot of literature has been done on natural convection and heat transfer in enclosures with the use of nanofluids, there are still a few areas that are understudied concerning inverted T-shaped geometries. The available literature has dealt with simple square, rectangular, or triangular cavities, whereas complex structures like inverted T-shaped enclosures have not been considered much, especially when hybrid nanofluids are used to fill them. Moreover, the synergistic effect of the Casson fluid model has never been effectively studied on this geometry. The impact of an inclined magnetic field (MHD) in regulating the structure of flow and heat conduction within such enclosures is also quite uninvestigated. Furthermore, the use of artificial intelligence, i.e., ANNs, to predict the performance of any thermal system and adjust the system parameters to the maximum, has not been implemented so far for this setup. Addressing these gaps would provide an opportunity to develop a more precise and generalized model of hybrid nanofluid heat transfer in solar-powered systems and other engineering applications.

1.1 *Objectives of the study*

The current study aims at explaining the phenomenon of magnetoconvective heat transfer and fluid flow inside an inverted T-shaped enclosure, which is filled with Casson hybrid nanofluid of multi-walled carbon nanotubes and iron oxide nanoparticles, with a view to the application in the solar thermal energy sector. This research has the objective of quantifying the effects of the buoyancy factor, the strength of a magnetic field, and non-Newtonian rheology on thermal performance with the finite element method and developing a model used as an artificial neural network that can effectively and quickly predict the subsequent thermal behaviour.

1.2 *Novelty of the study*

What is new in this work is the combined study of magnetoconvective heat transfer in the described geometry in the case of using a Casson hybrid nanofluid, with the addition of multi-walled carbon nanotubes and iron oxide nanoparticles. The study is also the first to integrate non-Newtonian rheology, hybrid nanofluid modelling, magnetic field impacts, and artificial neural network-based prediction into a single numerical model, thus providing new physical implications for the solar thermal energy storage and management systems.

1.3 *Limitations of the study*

The current study is limited to steady and laminar two-dimensional flow of the Casson hybrid nanofluid at constant material properties. The analysis excludes induced magnetic fields, Joule heating, and thermal radiation, turbulence, and experimental validation.

2. Mathematical formulation of the problem

The geometry that is considered is a T-shaped inverted cavity, as shown in Figure 1, with height L and width $W(L = W)$. The ratio of cavity is provided as $L_1/L = 0.2$. The enclosure has an occupancy of a hybrid nanofluid of Multi-Walled Carbon Nanotubes (MWCNTs) and iron oxide (Fe_3O_4) nanoparticles. The effect of an inclined magnetic field is studied in this work through the MHD model and the Casson fluid model. This structure has a practical application in solar energy systems, such as solar thermal systems, PV/T systems, and solar-assisted energy storage systems, whereby hybrid nanofluids have been used to enhance the efficiency of heat transfer.

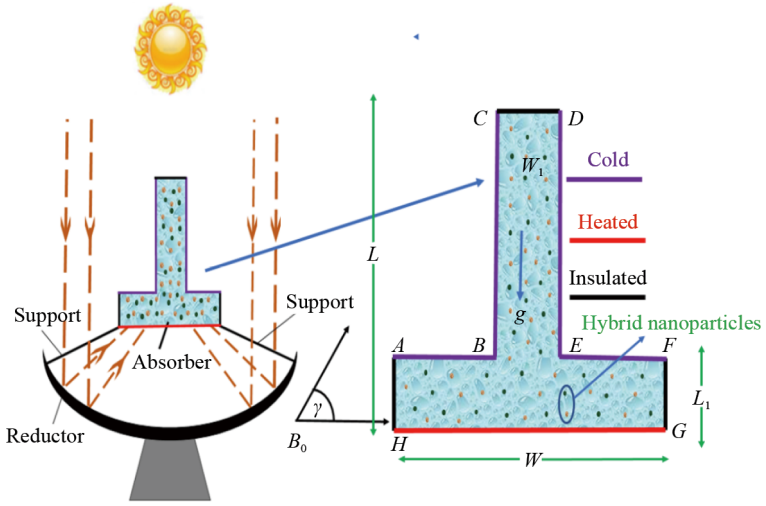

Figure 1. Problem configuration schematic

The governing equations for fluid flow and heat transfer are reduced after applying the assumptions as

$$\frac{\partial u}{\partial x}+\frac{\partial v}{\partial y}=0, \tag{1}$$

$$u\frac{\partial u}{\partial x}+v\frac{\partial u}{\partial y}=-\frac{1}{\rho_{hnf}}\frac{\partial p}{\partial x}+\frac{\mu_{hnf}}{\rho_{hnf}}\left(1+\frac{1}{\beta}\right)\left(\frac{\partial^2 u}{\partial x^2}+\frac{\partial^2 u}{\partial y^2}\right)-\frac{\sigma_{hnf}}{\rho_{hnf}}B_0^2\left(u\sin^2\gamma-v\cos\gamma\sin\gamma\right), \tag{2}$$

$$u\frac{\partial v}{\partial x}+v\frac{\partial v}{\partial y}=-\frac{1}{\rho_{hnf}}\frac{\partial p}{\partial y}+\frac{\mu_{hnf}}{\rho_{hnf}}\left(1+\frac{1}{\beta}\right)\left(\frac{\partial^2 v}{\partial x^2}+\frac{\partial^2 v}{\partial y^2}\right)+g\frac{(\rho\beta_{1\,\mathrm{T}})_{hnf}}{\rho_{hnf}}(T-T_{\mathrm{C}})$$

$$-\frac{\sigma_{hnf}}{\rho_{hnf}}B_0^2\left(V\cos^2\gamma-u\cos\gamma\sin\gamma\right), \tag{3}$$

$$u\frac{\partial T}{\partial x}+v\frac{\partial T}{\partial y}=\alpha_{hnf}\left(\frac{\partial^2 T}{\partial x^2}+\frac{\partial^2 T}{\partial y^2}\right). \tag{4}$$

Here, u and v represent the velocity components in the (x, y) plane, while g denotes gravitational acceleration. The thermophysical characteristics of the hybrid nanofluid are listed in Table 1 (refer to Ref. [35]).

2.1 *Boundary conditions*

The boundary conditions in the dimensional u and v coordinates are

$$\text{At AB, BC, DE, EF } T=T_c,\ u=v=0 \tag{5}$$

$$\text{At HG } T=T_h,\ u=v=0 \tag{6}$$

$$\text{At CD, AH, FG } \frac{\partial T}{\partial y} = 0. \tag{7}$$

The following parameters are used to non-dimensionalize governing equations:

$$(X^*, Y^*) = \left(\frac{x}{L}, \frac{y}{L}\right), \quad (U^*, V^*) = \left(\frac{u, v}{L}\right), \tag{8}$$

$$P^* = \frac{PL^2}{\rho_f \alpha_f \nu_f}, \quad \theta = \frac{T - T_c}{T_h - T_c}. \tag{9}$$

The governing equations can be written in dimensionless form as follows [35]:

$$\frac{\partial U^*}{\partial X^*} + \frac{\partial V^*}{\partial Y^*} = 0, \tag{10}$$

$$U^* \frac{\partial U^*}{\partial X^*} + V^* \frac{\partial U^*}{\partial Y^*} = -\frac{\partial P}{\partial X^*} + \frac{\mu_{hnf}/\mu_f}{\rho_{hnf}/\rho_f} \Pr \left(1 + \frac{1}{\beta}\right) \left(\frac{\partial^2 U^*}{\partial X^{*2}} + \frac{\partial^2 U^*}{\partial Y^{*2}}\right)$$
$$- \frac{\sigma_{hnf}/\sigma_f}{\rho_{hnf}/\rho_f} \Pr \mathrm{Ha}^2 \left(U^* \sin\gamma - V^* \cos\gamma\right), \tag{11}$$

$$U^* \frac{\partial V^*}{\partial X^*} + V^* \frac{\partial V^*}{\partial Y^*} = -\frac{\partial P}{\partial Y^*} + \frac{\mu_{hnf}/\mu_f}{\rho_{hnf}/\rho_f} \Pr \left(1 + \frac{1}{\beta}\right) \left(\frac{\partial^2 V^*}{\partial X^{*2}} + \frac{\partial^2 V^*}{\partial Y^{*2}}\right)$$
$$+ \frac{(\rho\beta_1)_{hnf}}{(\rho\beta_1)_f} \mathrm{Ra} \Pr \theta - \frac{\sigma_{hnf}/\sigma_f}{\rho_{hnf}/\rho_f} \Pr \mathrm{Ha}^2 \left(V^* \cos\gamma - U^* \sin\gamma\right), \tag{12}$$

$$U^* \frac{\partial \theta}{\partial X^*} + V^* \frac{\partial \theta}{\partial Y^*} = \frac{k_{hnf}/k_f}{(\rho c_p)_{hnf}/(\rho c_p)_f} \left(\frac{\partial^2 \theta}{\partial X^{*2}} + \frac{\partial^2 \theta}{\partial Y^{*2}}\right). \tag{13}$$

The physical parameters are represented by the following expressions:

$$\Pr = \frac{\nu_f}{\alpha_f}, \ \mathrm{Ra} = \frac{g\beta_{1f}(T_h - T_c)L^3}{\alpha_f \nu_f}, \ \mathrm{Ha} = BoL\sqrt{\frac{\sigma_f}{\rho_f \nu_f}}. \tag{14}$$

$$\frac{\alpha_{hnf}}{\alpha_f} = \frac{k_{hnf}/k_f}{(\rho c_p)_{hnf}/(\rho c_p)_f}, \quad \frac{\nu_{hnf}}{\nu_f} = \frac{\mu_{hnf}/\mu_f}{\rho_{hnf}/\rho_f}. \tag{15}$$

2.2 *Thermophysical correlations and properties of hybrid nanofluids*

Thermophysical correlations and properties of hybrid nanofluids are presented in Table 1 and Table 2.

Table 1. Physical properties of hybrid nanofluid [36, 37]

Characteristics	Fluid (Water)	Fe_3O_4	MWCNT	MWCNT-Fe_3O_4/water hybrid nanofluid
Pr	6.2	-	-	-
ρ (Kg/m^3)	998.5	5,180	2,100	1,002.34 ($\phi = 0.001$) 1,010.04 ($\phi = 0.003$)
β (K^{-1})	21	1.18×10^{-5}	2.84×10^{-4}	
k (W/mK)	0.602	17.65	3,000	0.6734 ($\phi = 0.001$) 0.6856 ($\phi = 0.003$)
c_p (j/KgK)	4,182	104	796	4,182.66 ($\phi = 0.001$) 4,183.99 ($\phi = 0.003$)
σ (s/m)	5.5×10^{-6}	1×10^5	300	-
$\mu \times 10^4$/kg/ms	8.55×10^{-4} kg/ms	-		-
v/mPas	0.79	-		0.91 ($\phi = 0.001$) 0.01 ($\phi = 0.003$)

Table 2. Thermophysical correlations of hybrid nanofluids [36, 37]

Properties	Hybrid nanofluid
Viscosity	$\frac{\mu_{hnf}}{\mu_{bf}} = \frac{1}{(1-\phi_{Fe_3O_4})^{2.5}(1-\phi_{MWCNT})^{2.5}}$
Density	$\frac{\rho_{hnf}}{\rho_{bf}} = \phi_{Fe_3O_4}\frac{\rho_{Fe_3O_4}}{\rho_{bf}} + \phi_{MWCNT}\frac{\rho_{MWCNT}}{\rho_{bf}} + (1-\phi_{Fe_3O_4}-\phi_{MWCNT})$
Thermal capacity	$\frac{(\rho c_p)_{hnf}}{(\rho c_p)_{bf}} = \phi_{Fe_3O_4}\frac{(\rho c_p)_{Fe_3O_4}}{(\rho c_p)_{bf}} + \phi_{MWCNT}\frac{(\rho c_p)_{MWCNT}}{(\rho c_p)_{bf}} + (1-\phi_{Fe_3O_4}-\phi_{MWCNT})$
Thermal conductivity	$\frac{k_{hnf}}{k_{bf}} = \frac{\frac{(\phi_{Fe_3O_4}k_{Fe_3O_4}+\phi_{MWCNT}k_{MWCNT})}{\phi_{Fe_3O_4}+\phi_{MWCNT}} + \left\{\begin{array}{l} 2k_{bf}+2(\phi_{Fe_3O_4}k_{Fe_3O_4}+\phi_{MWCNT}k_{MWCNT}) \\ -2(\phi_{Fe_3O_4}+\phi_{MWCNT})k_{bf}\end{array}\right\}}{\frac{(\phi_{Fe_3O_4}k_{Fe_3O_4}+\phi_{MWCNT}k_{MWCNT})}{\phi_{Fe_3O_4}+\phi_{MWCNT}} + \left\{\begin{array}{l} 2k_{bf}-(\phi_{Fe_3O_4}k_{Fe_3O_4}+\phi_{MWCNT}k_{MWCNT}) \\ +(\phi_{Fe_3O_4}+\phi_{MWCNT})k_{bf}\end{array}\right\}}$
Electrical conductivity	$\frac{\sigma_{hnf}}{\sigma_{bf}} = \frac{\frac{(\phi_{Fe_3O_4}\sigma_{Fe_3O_4}+\phi_{MWCNT}\sigma_{MWCNT})}{\phi_{Fe_3O_4}\phi_{MWCNT}} + \left\{\begin{array}{l} 2\sigma_{bf}+2(\phi_{Fe_3O_4}\sigma_{Fe_3O_4}+\phi_{MWCNT}\sigma_{MWCNT}) \\ -2(\phi_{Fe_3O_4}+\phi_{MWCNT})\sigma_{bf}\end{array}\right\}}{\frac{(\phi_{Fe_3O_4}k_{Fe_3O_4}+\phi_{MWCNT}k_{MWCNT})}{\phi_{Fe_3O_4}+\phi_{MWCNT}} + \left\{\begin{array}{l} 2\sigma_{bf}-(\phi_{Fe_3O_4}\sigma_{Fe_3O_4}+\phi_{MWCNT}\sigma_{MWCNT}) \\ +(\phi_{Fe_3O_4}+\phi_{MWCNT})\sigma_{bf}\end{array}\right\}}$

Quantity of engineering interest is the average Nusselt number (Nu_{avg}):

$$\text{Local Nusselt Number: } Nu(\eta)_{\text{local}} = -k_{hnf}\frac{\partial\theta}{\partial Y^*}. \tag{16}$$

$$\text{Average Nusselt Number: } Nu_{\text{avg}} = \frac{1}{S}\int_S Nu(\eta)_{\text{local}}\, d\eta. \tag{17}$$

3. Grid independence analysis and numerical code validation

A grid independence study was conducted to make sure that the numerical results are not mesh dependent and that they do not change with consecutive refinements. The evaluation was done by checking the average Nusselt number

(Nu_{avg}) at the varying levels of refinement in terms of the Number of Elements (NEL) and Degrees of Freedom (DOF). As can be seen in Table 3 and Table 4, the values of converge, with the value 15.81 becoming steady with Refinement Levels (R.L.) 8 and 9, as well as with no differences in the value of Nu_{avg} upon further refinement. It suggests that R.L. 8 has an ideal balance between accuracy and computational efficiency, which is sufficiently high to make accurate predictions. The extra-fine grid distribution adopted is shown in Figure 2. In order to further prove the plausibility of the computational model, a validation exercise was performed by juxtaposing the current results with benchmark studies reported by Mohebbi and Yuan [38]. A very good correspondence between the current predictions and earlier published data as the results, as shown in Figure 3, proves the strength and credibility of the created numerical framework. Table 2 compares values of Nusselt numbers (Nu_{avg}) as obtained in the current study with those obtained by [39, 40]. The values show a high level of concordance throughout the whole scale of Rayleigh numbers, with the difference being less than 0.02. This observation supports the accuracy and validity of the simulations used in this paper. As a result, the current numerical system is confirmed, and the current model proves to be able to exhibit the same thermal-convection properties that were previously studied.

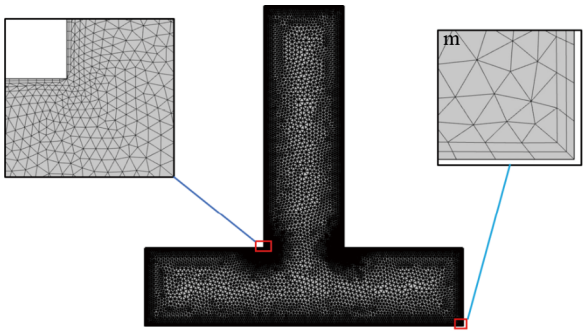

Figure 2. Discretized geometry of the problem

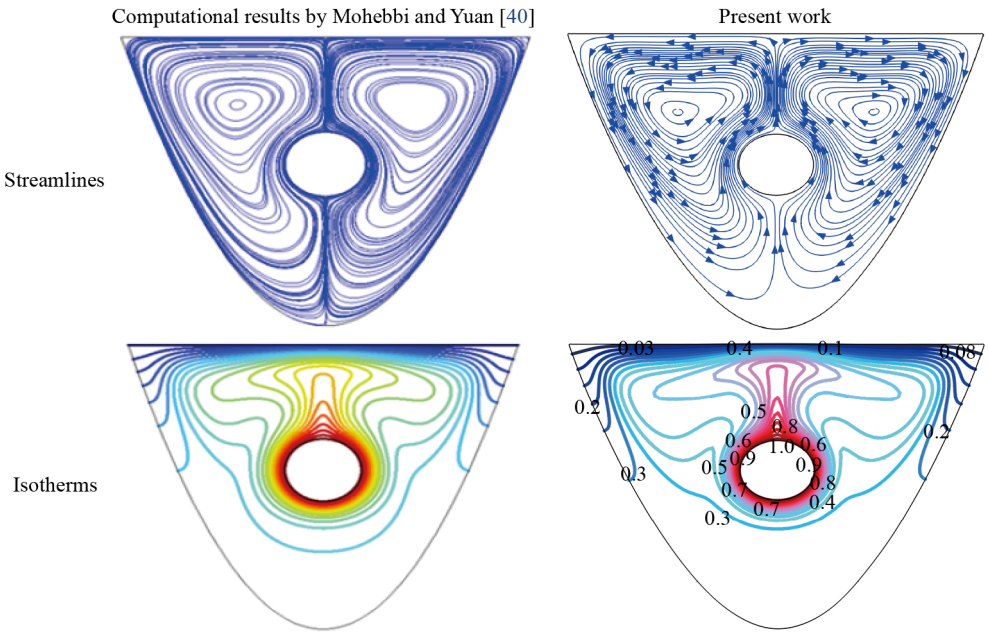

Figure 3. Assessment of present results in relation to the experimental and computational study of Mohebbi and Yuan [38]

Table 3. Illustrates the correspondence between the current results and earlier studies for the average Nusselt number (Nu_{avg})

Ra	Current study	Khanafer et al. [39]	Sheikholeslami et al. [40]
10^3	1.1191	1.1178	1.1432
10^4	2.2556	2.2449	2.2749
10^5	4.5345	4.5221	4.5199

Table 4. Mean heat transfer rates (Nusselt numbers) at successive refinement levels

Refinement level	D.O.F	NEL	Nu_{avg}
Extremely coarse	2,528	243	11.292
Coarser	5,678	591	11.627
Normal	13,121	1,532	11.753
Fine	20,112	2,365	11.767
Finer	52,606	6,479	11.780
Extra fine	132,602	16,968	11.783
Extremely fine	151,488	19,666	11.785

Table 5. Mean heat transfer coefficients (Nusselt numbers) at diverse parameter values

Ra	Ha	β	FEM (Nu_{avg})	ANN (Nu_{avg})	Abs_{Error}	Rel_{Error} (%)
10^3			7.4765	7.55	0.0735	0.98
10^4			7.4773	7.60	0.1227	1.64
10^5			11.783	11.95	0.167	1.42
	0		14.595	14.45	0.145	0.99
	20		11.783	11.70	0.083	0.70
	50		7.6017	7.63	0.0283	0.37
		0.01	7.4765	7.55	0.0735	0.98
		1	11.783	11.90	0.117	0.99
		10	14.649	14.55	0.099	0.68

Table 5 compares the average Nusselt numbers (Nu_{avg}) obtained from FEM simulations and ANN predictions for varying Rayleigh numbers (Ra), Hartmann numbers (Ha), and Casson fluid parameters (β). The Rayleigh number, which measures the intensity of the buoyancy-driven convection, exhibits a significant increase of the heat transfer by increasing the Rayleigh number between the values of 10^3 and 10^5. The values of the ANN perfectly follow the same pattern, and thus, the ability of the ANN to reflect the effects of the thermal buoyancy in the convective flow is confirmed. The Hartmann number, a measure of the effect of an imposed magnetic field, dampens the fluid motion through Lorentz forces; an increase in the magnitude of Ha reduces the values of the Nu_{avg}, which reflects the damping of the convective currents, which is also accurately reflected by the ANN predictions. The Casson parameter of the fluid is denoted by the β parameter, indicating that the higher the beta, the higher the yield stress of the fluid and the lower the effective mobility of the fluid. This leads to small changes in the values of the Nu_{avg}, which the ANN can capture satisfactorily, as it is sensitive to the rheological characteristics of the fluid. The absolute errors (0.0283-0.167) and relative errors (< 2) show that the ANN is not only capable of restating the quantitative FEM results but also displays the actual underlying physical process of heat transfer, that is, enhancing buoyancy with increasing Ra, suppressing magnetism with Ha, and modulating rheology with beta. The results indicate that the ANN can be used as an effective predictive method to examine the complicated magneto-convective heat transfer in non-Newtonian fluids to provide physical information with minimum computing cost.

4. ANN

An ANN is an artificial brain model that models the human brain, which can model nonlinear relationships and give precise predictive modelling of engineering problems. In the given work, a feed-forward backpropagation ANN has been used due to its effectiveness in the area of mapping of finite input-output relationships. The network was designed (Figure 4) to take three input parameters, Rayleigh number, Hartmann number, and Casson parameter and one output variable temperature according to a 6,144 sample size dataset of known validated simulations. Two hidden layers with 10 neurons each were adopted to successfully model nonlinearities of the systems and thus provided a balance between prediction accuracy and computational cost. The training was carried out via the Levenberg Marquardt (LM) algorithm that is known to converge relatively quickly in medium networks, with the dataset split into training (80 percent), validation (10%), and testing (10%) subsets. Moreover, there was the use of early stopping to avoid overfitting with an effective convergence at epoch 332 (Figure 5). The model performance was also properly tested diagnostically: the Mean Squared Error (MSE) curve showed a steady downward trend in all subsets, the error histogram had a tight distribution with its main part near zero (Figure 6), strong agreement is observed (Figure 7), and regeneration plots showed that correlation coefficients were close to one, thus confirming excellent predictive accuracy (Figure 8). Convergence analysis also showed that there was a gradual decrease in the gradient to 9.37 times 10^{-8}, the damping (mu) parameter is also reduced to 1 times 10^{-9} (Figure 9), and there is also a limited check of validation (4), which showed reliable training without overfitting. On the whole, the designed ANN model, which consisted of four inputs, two hidden layers, and one output neuron, turned out to be a powerful and computationally efficient surrogate modeling tool, thus highly efficient in real-time thermal analysis, optimization, and sensitivity studies in magnetoconvective heat transfer of non-Newtonian fluids in porous media [5, 41, 42].

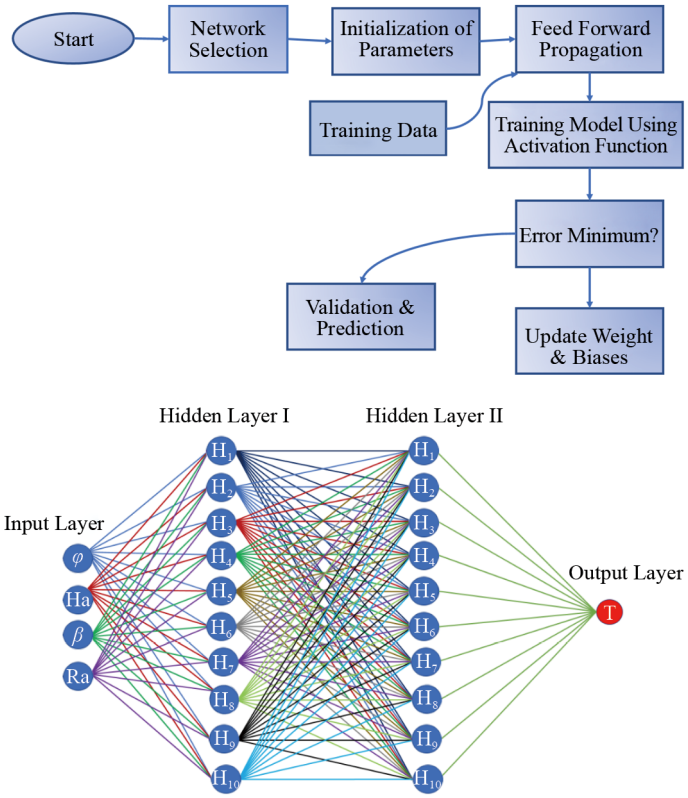

Figure 4. Architecture and workflow of an ANN

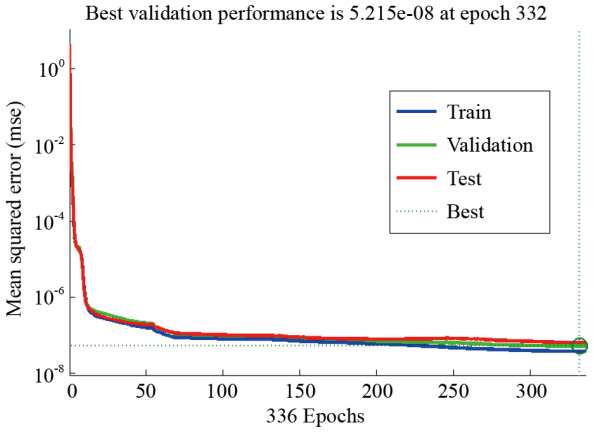

Figure 5. Variation in MSE for training, validation, and testing sets throughout the training epochs

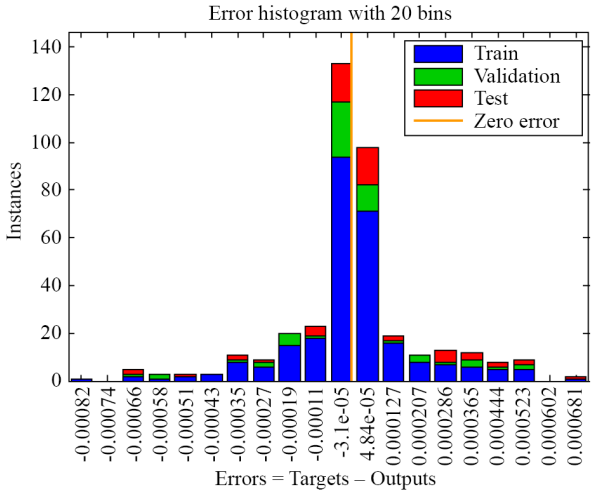

Figure 6. Visualization of the error distribution for the BRT-ANN model

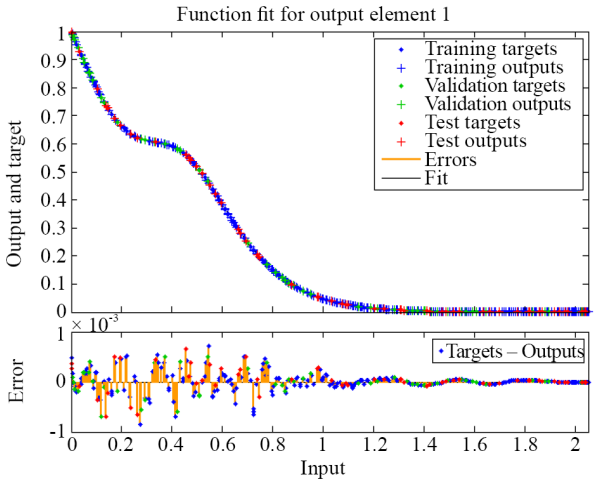

Figure 7. Curve fitting graph

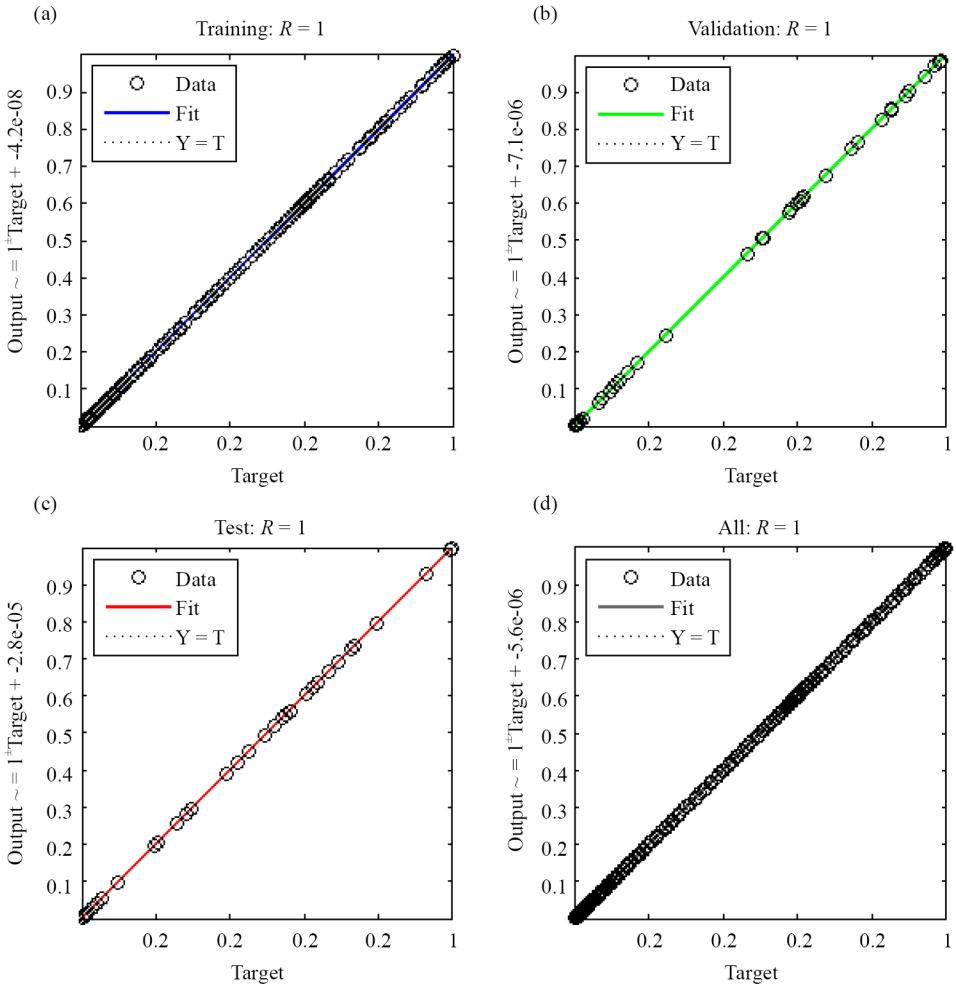

Figure 8. Regression analysis visualization for the BRT-ANN model

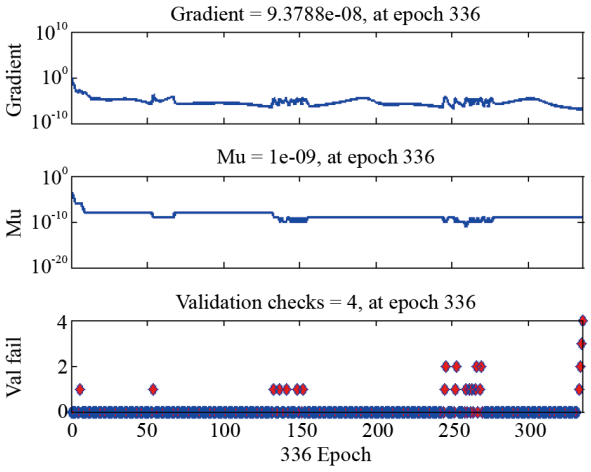

Figure 9. Training performance of the ANN model showing the gradient, damping parameter (mu), and validation checks across 8 epochs, indicating stable convergence and no overfitting

5. Description of outcomes

This paper explores the thermophysical characteristics of a hybrid nanofluid consisting of iron oxide and MWCNTs in a T-shaped permeable enclosure for solar energy use. The FEM was used in COMSOL Multiphysics to perform numerical simulations. The parametric analysis involved the Rayleigh number (10^3-10^5) and Hartmann number (0-50), nanoparticles concentration (0-0.05), and the magnetic field inclination angle (0-90) in constant ratios, keeping the Prandtl number (Pr = 6.8). These parameters and how they affect the flow and thermal transport properties are investigated by streamline and isotherm distributions. Also, global and local thermal performance measures such as the average and local Nusselt numbers, entropy generation, and Bejan number are evaluated to measure the extent to which the enhancement of heat transfer is achieved, the minimization of entropy, and general thermodynamic effectiveness.

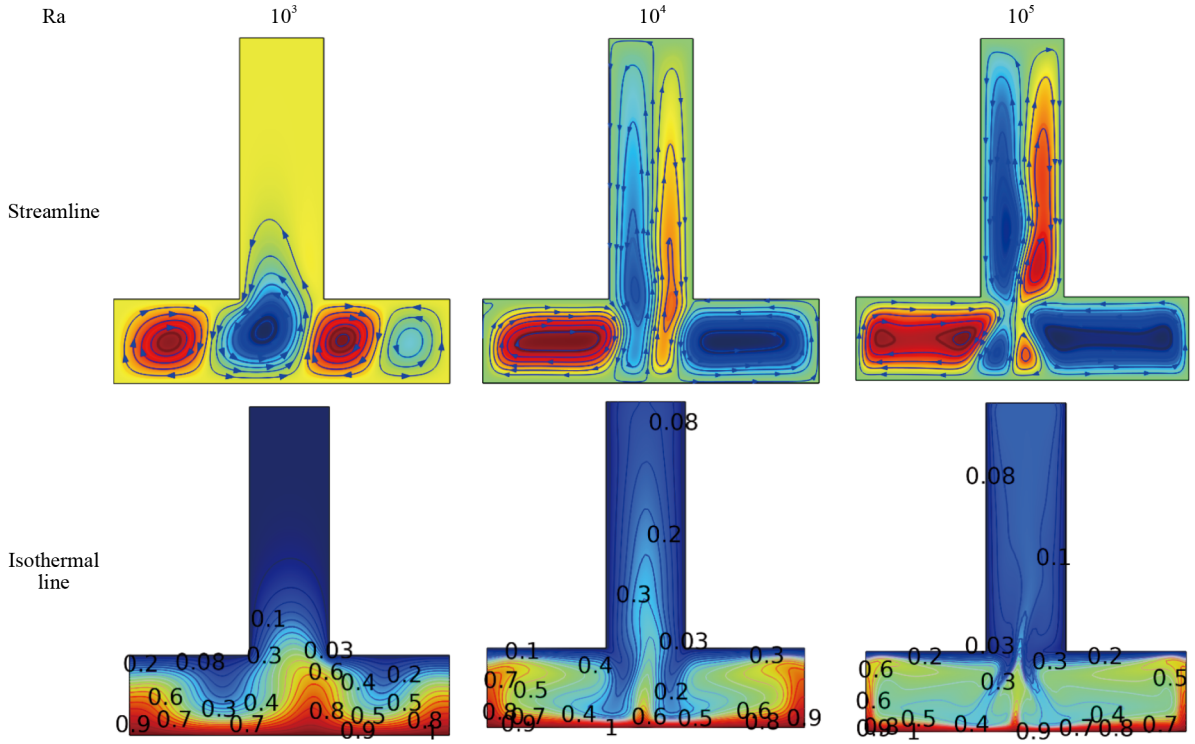

Figure 10. Influence of Ra on the streamlines and isotherms

As shown in Figure 10, the Rayleigh number's influence on the distributions of streamlines and isothermal lines marks the transition from conduction-dominated heat transfer to convection-dominated heat transfer. At Ra = 10^3 the streamlines indicate the weak buoyancy-driven flow with a single primary vortex, indicative of conduction as the primary mode of heat transfer. The isothermal lines are almost parallel to one another, suggesting a thick thermal boundary layer with negligible convective mixing. As Ra increases to 10^4, this emphasizes the strengthening of circulation with the flow forming larger vortices and improved movement of fluids. The isothermal lines are gradually bent, signifying the enhancement of convective transport, while the thermal boundary layer commences thinning. At Ra = 10^5, the streamlines demonstrate multiple vortices with strong recirculating zones, indicating vigorous convection. The isothermal lines are severely distorted to indicate good thermal mixing and the significant lessening of the thermal boundary layer thickness; this progressive alteration with increasing Ra indicates that natural convection dominates heat transfer, which is enhanced by greater buoyant forces, promotes fluid motion and thermal energy transfer.

Figure 11 illustrates the streamline and isothermal line distributions for varying values of the parameter β (0.01, 1, and 10). The first row showcases the streamline patterns, whereas the second row represents the temperature distribution

using isothermal lines. As β increases to 1, the strength of the flow becomes very high, and the bottom region develops various vortices. The streamline patterns show increased convective movement, and this increases mixing of hot and cold areas. In this way, the isothermal line is more deformed, which refers to the more significant part of hollows, played by convection in heat transfer. At $\beta = 10$, the convective motion is very strong, and there is the development of a lot of extremely strong vortices in the vicinity of the hot region. The streamlines reveal that there is effective flow circulation, and this enhances convection in heat transfer. The isothermal lines have an accelerated temperature gradient close to the heated surface, and this indicates a high exchange of heat caused by the enhanced buoyancy-facilitated flow. The identified changes are attributed to the fact that the value of β increases, thereby enhancing the effect of buoyancy, which makes natural convection stronger. When β is lower, the heat mechanism is dominated by conduction because there is not much buoyancy action. With an increase in β, the influence of the natural convection has a greater effect, where the fluid motion becomes very high, and a maximum enhancement of heat transfer occurs. These findings are critical to the shift between the conduction-controlled heat transfer and the convection-dominated heat transfer.

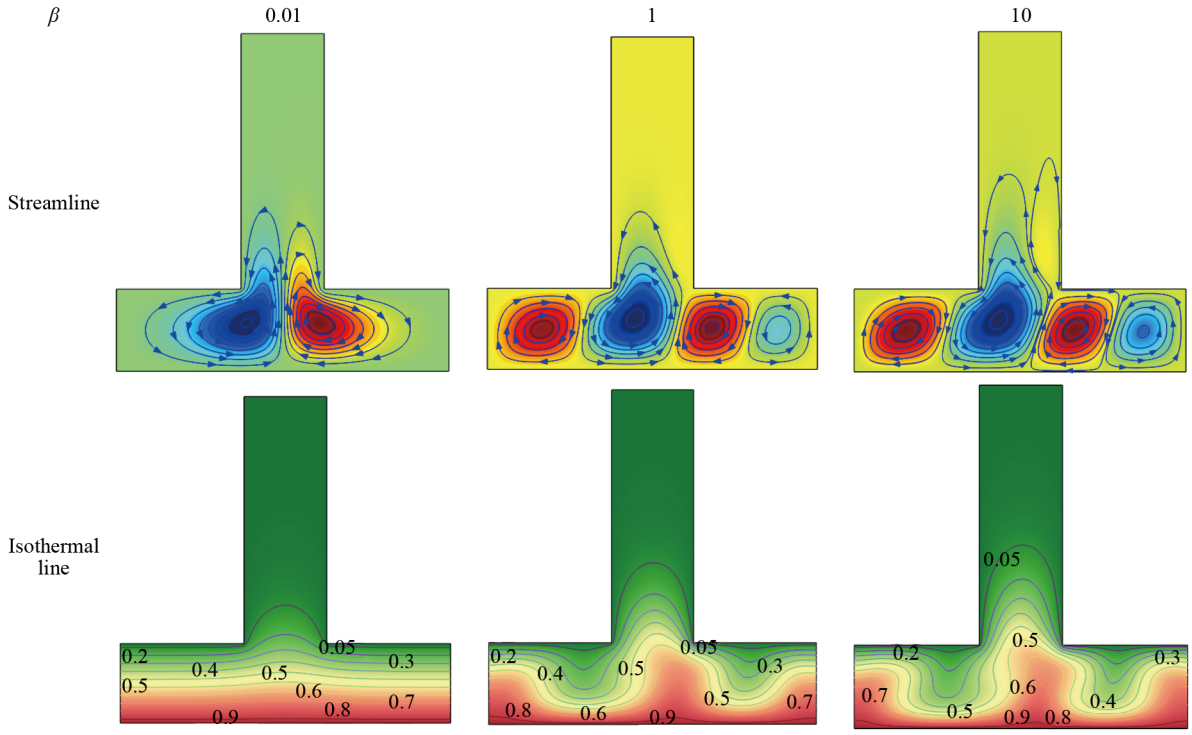

Figure 11. Streamline and isotherm behavior with different β

The above Figure 12 shows that increasing the Ha affects the flow and heat transfer in a T-shaped cavity and causes a change in modes of transfer between convection-dominated and conduction dominated. A magnetic field is absent at Ha = 0, and thus convection is easy and multiple vortices are developed around the heated region, leading to good thermal mixing. The steep gradients of isothermal lines in this case point to the dominance of convection. When Ha becomes 20, the Lorentz force opposes fluid flow and makes the vortex weak, reducing the vortex intensity, yielding to sinusoidal isothermal lines, which are smooth, showing the trend towards conduction. At Ha = 50, the magnetic field greatly damps circulation and makes the isothermal lines stratified; this is because the heat transfer is conducted by the magnetic field. The magnetic field has the effect of suppressing the buoyancy-driven fluid flow, which minimizes the role of thermal mixing and convective transport. This evidence shows that amplification of Ha indeed manages the fluid flow and changes the heat exchange properties; this is of essence in MHD systems like thermal management as well as industrial cooling systems.

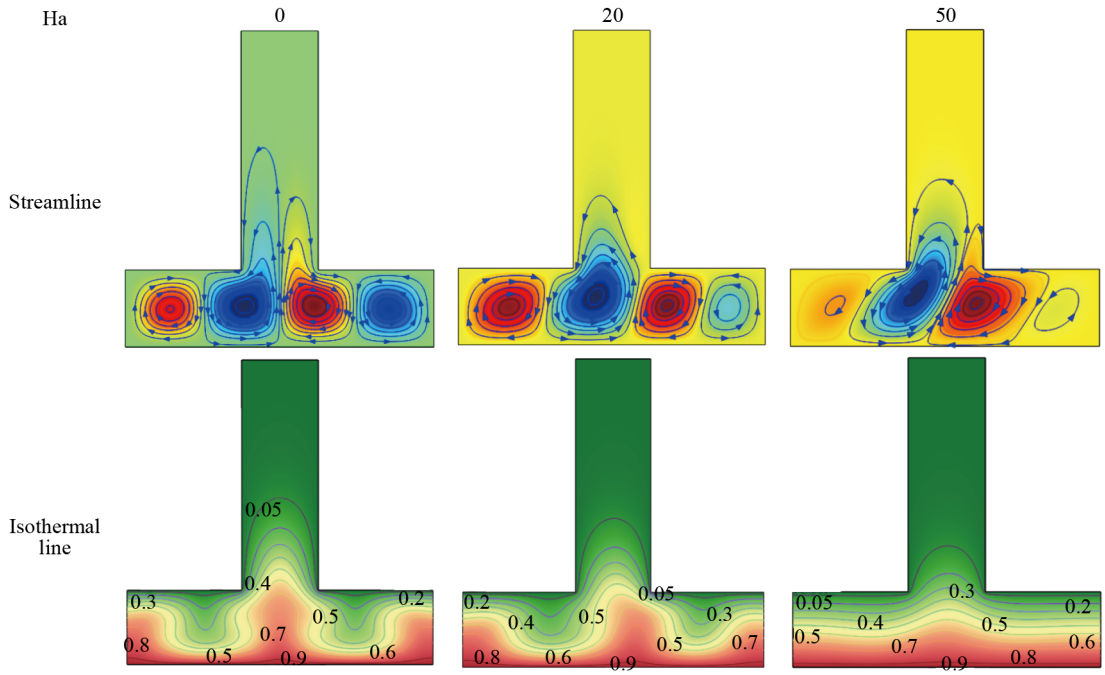

Figure 12. Streamline and isotherm patterns for different Ha values

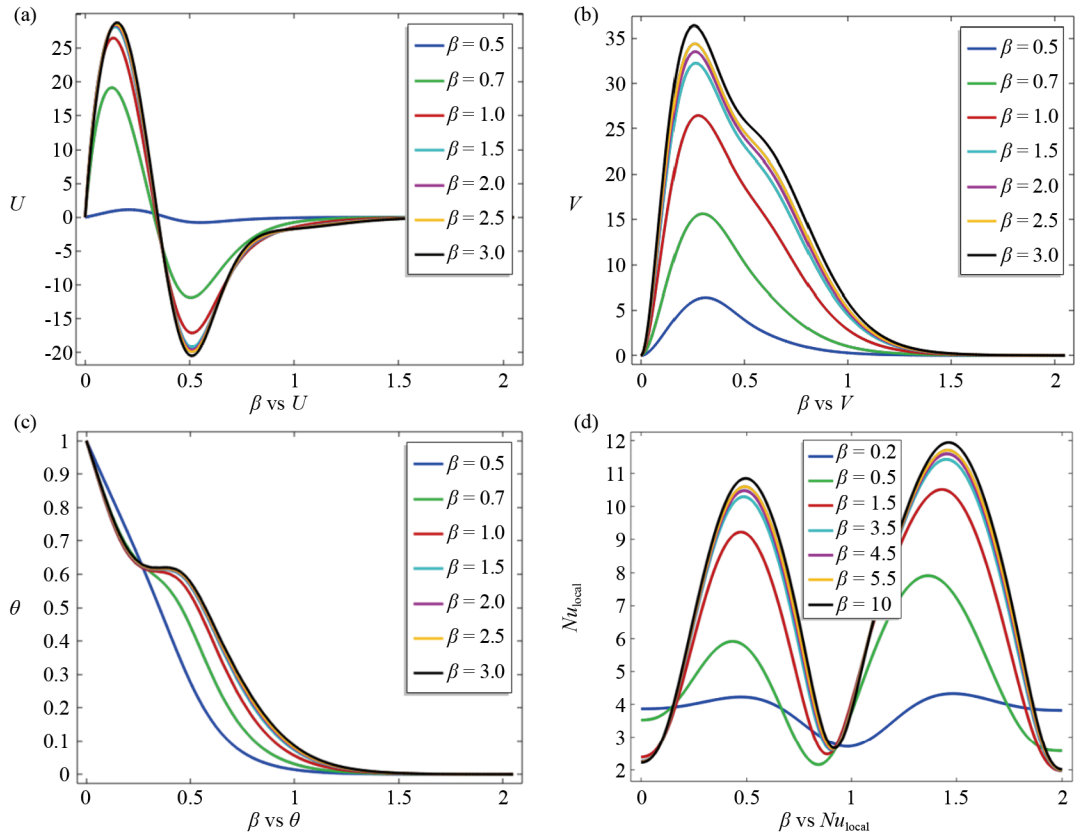

Figure 13. Represents the effect of β on velocity, temperature, and local Nusselt number

Figure 13a-b shows how the Casson fluid parameter of the fluid (parameter of the fluid) is influenced by the velocity components (U, V), temperature (θ), and local Nusselt number (Nu_{local}). At lower values of β, the non-Newtonian forces are strong, and the velocity peaks become sharper in both directions since the resistance to deformation is decreased, whereas with higher values of β, fluid motion is inhibited and the curves become flat like those of Newtonian behaviour. As weaker convection enables larger amounts of heat to be trapped in the boundary layer, the temperature profile increases as the value of the nusselt number rises and the local Nusselt number increases, which is the best indication of the increased heat transfer among the convectional activity. Physically, it implies that a higher value of heat transfer is encouraged while fluid movement is inhibited by greater values of β. This can be directly applied to solar thermal systems and solar collectors, where the control of the value of β can be used to optimize the trade-off between heat absorption and convection to enhance storage of energy and efficiency of energy conversion.

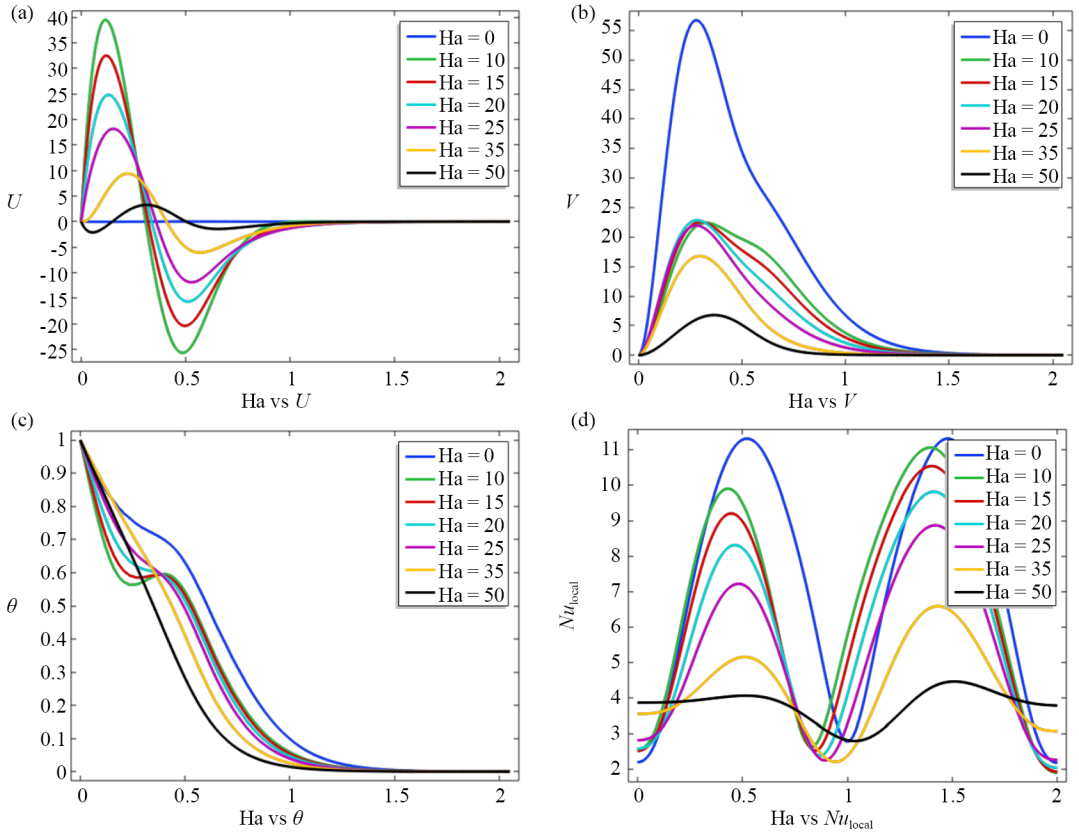

Figure 14. Represents the effect of Hartmann number Ha on velocity, temperature, and local Nusselt number

Figure 14a illustrates the impact of Ha on the velocity component along the U-direction. It is observed that as Ha increases, the peak velocity along this direction decreases significantly. This trend can be attributed to the growing influence of the Lorentz force, which acts as a damping force resisting fluid motion. When Ha = 0, the fluid flows more freely due to the absence of a magnetic field. However, as Ha increases up to 50, the flow becomes increasingly restricted, resulting in a flattened and broadened velocity profile with lower maximum values. This clearly indicates that the applied magnetic field suppresses the forward motion of the conducting fluid. Figure 14b shows the variation of velocity along the V-direction under the influence of different Ha values. Similar to the U-component, the transverse velocity is also reduced as Ha increases. However, the suppression in this direction is more uniform. The magnetic field provides a stabilizing effect across both components of velocity, limiting disturbances and fluctuations in the flow field. This stabilizing behavior is crucial for maintaining laminar flow conditions in magnetically controlled systems. In Figure 14c, the temperature

distribution θ is depicted as a function of Ha. As the magnetic field strength increases, the temperature throughout the fluid domain also increases. This can be explained by the fact that a stronger magnetic field suppresses the velocity, thereby reducing convective heat transport. With weaker convection, thermal diffusion becomes dominant, resulting in thicker thermal boundary layers and higher fluid temperatures. This behavior is especially evident near the heated surface, where temperature gradients become less steep as Ha increases. Figure 14d illustrates the variation in the local Nusselt number with increasing a. A clear decreasing trend is observed, signifying a reduction in the rate of convective heat transfer at the surface. This is a direct consequence of the magnetic field's damping effect on fluid motion. As the Lorentz force becomes stronger, the fluid's ability to transfer heat via convection diminishes, leading to lower Nusselt numbers. This result emphasizes the trade-off between magnetic control and thermal performance applications.

6. Conclusion

In this study, an ANN in combination with FEM modeling was used to explore magnetoconvective heat transfer in non-Newtonian Casson fluids, which has applications in solar thermal systems. The results provide a number of important physical observations:

1. By increasing the Casson fluid parameter, which is a measure of non-Newtonian behaviour, the domineering heat transfer process in conduction is replaced by the convection process. The result of this transition is an amplification of vortical circulation, increase of flow caused by buoyancy and enhanced dispersion of thermal energy within the fluid space.

2. Natural convection increases with increasing Rayleigh numbers that measure thermal buoyancy. The resulting outcome is an increase in the intensity of fluid movement, enhancement of vortical structures, reduced thermal boundary layers along the walls of the heated surfaces, and an increase in the efficiency of heat transfer.

3. The addition of a stronger magnetic field, in a form of the Hartmann number, decreases motion of the fluid by the Lorentz force. Such blocking reduces the intensity of convective currents and consequently reduces the total rate of heat transfer of the system.

4. When increasing the Casson fluid parameter r, the fluid tends towards the traits of a Newtonian fluid, where it allows easy transportation of heat through convective circulation and thus leads to a better performance of the whole system of heat transfer.

5. The magnetoconvective heat transfer is complex and nonlinear behaviour that was well represented by the two-hiding-layer feed-forward ANN. Its predictions were very close to FEM simulations, showing high precision, convergence and poor overfitting.

6. ANN and FEM applied synergistically provide a powerful platform of real-time thermal analysis, optimisation and sensitivity studies. The combination method is used to effectively explore the effect of fluid properties, magnetic fields, and buoyancy effects on convective heat transfer in solar thermal systems.

7. Applications of the present study

The results of the present study have direct implications on the design and optimisation of solar thermal energy storage systems, where the critical factors of improving the performance are the efficient heat transfer and magnetic control. The demonstrated ability to control the convective transfer of heat through magnetic fields enables effective thermal control of solar collectors, thermal batteries and heat exchangers that utilize electrically conducting hybrid nanofluids. Additionally, the addition of non-Newtonian rheological effects provides useful information on the optimization of fluid recipes in the high-technology cooling systems, including electronic cooling, nuclear reactor safety systems, and miniature energy devices. The tested ANN-based surrogate model also supports a quick prediction and optimisation, which makes the proposed framework relevant in the context of real-time control, system design, and optimisation of the parametric with the aim of renewable energy application i.e. magnetically controlled hybrid nanofluid flows.

8. Future scope

Future studies can focus on the study of transient and three-dimensional magnetoconvective flows in hybrid nanofluids, wherein other species of nanoparticles or ternary mixtures are added. Combining optimisation techniques with ANN surrogate models, optimized via the Levenberg-Marquardt algorithm might allow real-time forecast and regulation, thereby enhancing the design of advanced solar-thermal energy systems.

Acknowledgements

Authors M. Sarwar, N. Fatima and K. Abodayeh are thankful to Prince Sultan University for APC and support through TAS research lab.

Conflict of interest

The authors state that they do not have any conflicts of interest.

References

[1] Hachicha AA. On the use of hybrid nanofluids in direct absorption parabolic trough solar collector. *Renewable Energy*. 2025; 248: 123056.

[2] Huminic G, Huminic A, Fleacă C, Dumitrache F. Hybrid nanofluids-based direct absorption solar collector: An experimental approach. *International Journal of Thermophysics*. 2025; 46(3): 32.

[3] Kalsi S, Kumar S, Kumar A, Alam T, Sharma A, Yadav AS. A review on hybrid nanofluids for heat transfer: Advancements, synthesis, challenges and applications. *Discover Applied Sciences*. 2025; 7(7): 698.

[4] Hannoura AA, Shalaby SM, Ali N. Exploration and enhancement of the thermal properties of heat transfer fluids used in solar collectors. *Journal of Thermal Analysis and Calorimetry*. 2025; 150(25): 20799-20813.

[5] Rehman KU, Shatanawi W, Asghar Z, Kasim ARM. Neural networking analysis of thermally magnetized mass transfer coefficient (MTC) for Carreau fluid flow: A comparative study. *International Journal of Thermofluids*. 2025; 26: 101069.

[6] Matori A, Mohebbi R, Hashemi Z, Ma Y. Lattice Boltzmann study of multi-walled carbon nanotube (MWCNT)-Fe_3O_4/water hybrid nanofluids natural convection heat transfer in a Π-shaped cavity equipped by hot obstacle. *Journal of Thermal Analysis and Calorimetry*. 2019; 136: 2495-2508.

[7] Oztop HF, Oztop M, Varol Y. Numerical simulation of magnetohydrodynamic buoyancy-induced flow in a non-isothermally heated square enclosure. *Communications in Nonlinear Science and Numerical Simulation*. 2009; 14(3): 770-778.

[8] Kefayati GHR, Tang H. MHD thermosolutal natural convection and entropy generation of Carreau fluid in a heated enclosure with two inner circular cold cylinders, using LBM. *International Journal of Heat and Mass Transfer*. 2018; 126: 508-530.

[9] Turkyilmazoglu M, Alotaibi A. Analysis of MHD Stokes fluid flow in a cavity driven by moving parallel lid(s). *Theoretical and Computational Fluid Dynamics*. 2025; 39(4): 31.

[10] Alomari MA, Al-Farhany K, Al-Salami QH, Al-Jaburi K, Alyousuf FQA, Ali IR, et al. Magnetohydrodynamic mixed convection in lid-driven curvilinear enclosure with nanofluid and partial porous layer. *Journal of Magnetism and Magnetic Materials*. 2023; 582: 170952.

[11] Belhaj S, Ben-Beya B. Thermal performance analysis of hybrid nanofluid natural convection in a square cavity containing an elliptical obstacle under variable magnetic field. *International Journal of Numerical Methods for Heat and Fluid Flow*. 2022; 32(6): 1825-1860.

[12] Priyadharshini P, Sowndharya M. Predictive modeling of heat and mass transfer in MHD Casson nanofluid flow for solar collector applications. *Journal of Nanofluids*. 2025; 14(3): 339-350.

[13] Turkyilmazoglu M, Alotaibi A. On the viscous flow through a porous-walled pipe: Asymptotic MHD effects. *Microfluidics and Nanofluidics*. 2025; 29(6): 33.
[14] Negi AS, Rawat A, Monika, Bisht T, Rawat Y. Heat and mass transfer on MHD flow with hybrid nanofluids inside multi-tube system. *Journal of Thermal Analysis and Calorimetry*. 2025; 150(7): 2773-2789.
[15] David V, Chandran BDG, Meyrand R, Squire J, Yerger EL. Generalized expanding-box formulations of reduced magnetohydrodynamics in the solar wind. *Journal of Plasma Physics*. 2025; 91(2): 68.
[16] Turkyilmazoglu M, Alotaibi A. MHD front and rear stagnation-point flow of a moving permeable flat surface. *Physica D: Nonlinear Phenomena*. 2025; 471: 135075.
[17] Izadi M, Mohebbi R, Delouei AA, Sajjadi H. Natural convection of a magnetizable hybrid nanofluid inside a porous enclosure subjected to two variable magnetic fields. *International Journal of Mechanical Sciences*. 2019; 151: 154-169.
[18] Beckermann C, Ramadhyani S, Viskanta R. Natural convection flow and heat transfer between a fluid layer and a porous layer inside a rectangular enclosure. *Journal of Heat Transfer*. 1987; 109(2): 363-370.
[19] Baytaş AC, Liaqat A, Groşan T, Pop I. Conjugate natural convection in a square porous cavity. *Heat and Mass Transfer*. 2001; 37(4): 467-473.
[20] Chamkha AJ, Ismael MA. Conjugate heat transfer in a porous cavity filled with nanofluids and heated by a triangular thick wall. *International Journal of Thermal Sciences*. 2013; 67: 135-151.
[21] Bourantas GC, Skouras ED, Loukopoulos VC, Burganos VN. Heat transfer and natural convection of nanofluids in porous media. *European Journal of Mechanics B/Fluids*. 2014; 43: 45-56.
[22] Hajipour M, Dehkordi AM. Mixed-convection flow of Al_2O_3-H_2O nanofluid in a channel partially filled with porous metal foam: Experimental and numerical study. *Experimental Thermal and Fluid Science*. 2014; 53: 49-56.
[23] Nguyen MT, Aly AM, Lee SW. Natural convection in a non-Darcy porous cavity filled with Cu-water nanofluid using the characteristic-based split procedure in finite-element method. *Numerical Heat Transfer, Part A: Applications*. 2015; 67(2): 224-247.
[24] Al-Zamily AMJ. Analysis of natural convection and entropy generation in a cavity filled with multi-layers of porous medium and nanofluid with a heat generation. *International Journal of Heat and Mass Transfer*. 2017; 106: 1218-1231.
[25] Sheikholeslami M, Shamlooei M. Convective flow of nanofluid inside a lid driven porous cavity using CVFEM. *Physica B: Condensed Matter*. 2017; 521: 239-250.
[26] Sushma S, Pavithra CG, Gowtham KJ, Gireesha BJ. Impact of similarity transformations on hybrid nanofluid thermal behavior with thermal radiation on nonlinear stretching surface via Hermite wavelet transformations. *Radiation Effects and Defects in Solids*. 2024; 179: 1-25.
[27] Ali K, Ahmad S, Ahmad S, Tayebi T. Impact of magnetic field localization on the vortex generation in hybrid nanofluid flow. *Journal of Thermal Analysis and Calorimetry*. 2023; 148(13): 6283-6300.
[28] Mandal DK, Biswas N, Manna NK, Gorla RSR, Chamkha AJ. Hybrid nanofluid magnetohydrodynamic mixed convection in a novel W-shaped porous system. *International Journal of Numerical Methods for Heat and Fluid Flow*. 2023; 33(2): 510-544.
[29] Park YS, Lek S. Artificial neural networks: Multilayer perceptron for ecological modeling. In: *Developments in Environmental Modelling*. Amsterdam, Netherlands: Elsevier; 2016. p.123-140.
[30] Myers J, de Souza CR, Borghi-Silva A, Guazzi M, Chase P, Bensimhon D, et al. A neural network approach to predicting outcomes in heart failure using cardiopulmonary exercise testing. *International Journal of Cardiology*. 2014; 171(2): 265-269.
[31] Nagy B, Galata DL, Farkas A, Nagy ZK. Application of artificial neural networks in the process analytical technology of pharmaceutical manufacturing-a review. *The AAPS Journal*. 2022; 24(4): 74.
[32] Shafiq A, Çolak AB, Sindhu TN. Designing artificial neural network of nanoparticle diameter and solid-fluid interfacial layer on single-walled carbon nanotubes/ethylene glycol nanofluid flow on thin slendering needles. *International Journal for Numerical Methods in Fluids*. 2021; 93(12): 3384-3404.
[33] Mitusch SK, Funke SW, Kuchta M. Hybrid FEM-NN models: Combining artificial neural networks with the finite element method. *Journal of Computational Physics*. 2021; 446: 110651.
[34] Ahmadi MH, Tatar A, Seifaddini P, Ghazvini M, Ghasempour R, Sheremet MA. Thermal conductivity and dynamic viscosity modeling of Fe_2O_3/water nanofluid by applying various connectionist approaches. *Numerical Heat Transfer, Part A: Applications*. 2018; 74(6): 1301-1322.

[35] Parvin S, Roy NC, Saha LK. Magnetohydrodynamic natural convection of a hybrid nanofluid from a sinusoidal wavy cylinder placed in a curve-shaped cavity. *AIP Advances*. 2021; 11(8): 085029.
[36] Dong X, Lu Y, Li Y, Yang D. Quantification of mutual mass transfer coupled with heat transfer for CO_2/C_3H_8-heavy oil systems under reservoir conditions. *SPE Journal*. 2025; 30(3): 1432-1448.
[37] Yang S, Li L, Wang B, Zheng Y, Lund P, Wang J, et al. Modelling of radiative and convective heat transfer in an open cavity volumetric receiver for a 50-MW_{th} beam-down integrated receiver-storage concentrating solar thermal system. *Renewable Energy*. 2025; 242: 122457.
[38] Mohebbi R, Ma Y. Hybrid nanoparticle-enhanced fluid flow and heat transfer behaviors in a parabolic cavity with a heat source. *Arabian Journal for Science and Engineering*. 2025; 50(6): 4197-4207.
[39] Khanafer K, Vafai K, Lightstone M. Buoyancy-driven heat transfer enhancement in a two-dimensional enclosure utilizing nanofluids. *International Journal of Heat and Mass Transfer*. 2003; 46(19): 3639-3653.
[40] Sheikholeslami M, Gorji-Bandpy M, Soleimani S. Two phase simulation of nanofluid flow and heat transfer using heatline analysis. *International Communications in Heat and Mass Transfer*. 2013; 47: 73-81.
[41] Kousar N, Rehman KU, Fatima N, Shatanawi W, Asghar Z. Neural networking analysis on heat transfer in Casson fluid with mixed convection equipped in staggered cavity with anti-parallel moving boundary. *International Journal of Thermofluids*. 2025; 26: 101053.
[42] Rehman KU, Shatanawi W, Yian LY. Artificial intelligence based analysis for magnetized Casson fluid in partially heated cavity rooted with heated fin. *International Journal of Thermofluids*. 2025; 26: 101095.